Polímeros
ISSN 1678-5169 (Online)

https://doi.org/10.1590/0104-1428.20220050

ORIGINAL ARTICLE

Polyurethane/single wall carbon nanotube/ polymethylmethacrylate nanocomposite: PM3 semi-empirical method, Monte Carlo applied

Juan Ramon Campos-Cruz[1], Norma Aurea Rangel-Vázquez[1]*, Rosa Elvira Zavala-Arce[2] and Edgar Márquez-Brazon[3]

[1]División de Estudios de Posgrado e Investigación, Instituto Tecnológico de Aguascalientes, Aguascalientes, Aguascalientes, México

[2]División de Estudios de Posgrado e Investigación, Instituto Tecnológico de Toluca, Metepec, Estado do México, México

[3]Departamento de Química y Biología, Universidad del Norte, Barranquilla, Colombia

**norma.rv@aguascalientes.tecnm.mx*

Abstract

Firstly, this work shows the crosslinking of the Polyurethane/Single Wall Carbon Nanotube/ Polymethyl Methacrylate (PU/SWCNT/PMMA) nanocomposite at 298.15K using the PM3 semi-empirical method (Parameterized Model number 3), where the reaction was spontaneous and endothermic. The log P indicated a hydrophobic character. Subsequently, the Monte Carlo simulation was carried out at 303.15, 313.15 and 323.15K, where the Gibbs free energy and the dipole moment increased. However, the reactions were spontaneous and endothermic. The log P had hydrophobic character. Additionally, the entropy decreased due to the increase in intermolecular forces in the nanocomposite. Furthermore, FTIR analysis had similar vibrational frequencies, which was verified with the electronic distribution. Thus, this nanocomposite would have excellent physical and thermal stability, and it does not have reactions to polar solvents such as water so that it could be used in the human body.

Keywords: *PU, SWCNT, PMMA, PM3, Monte Carlo.*

How to cite: Campos-Cruz, J. R., Rangel-Vázquez, N. A., Zavala-Arce, R. E., & Márquez-Brazon, E. (2022). Polyurethane/single wall carbon nanotube/polymethylmethacrylate nanocomposite: PM3 semi-empirical method, Monte Carlo applied. *Polímeros: Ciência e Tecnologia*, *32*(3), e2022027. https://doi.org/10.1590/0104-1428.20220050

1. Introduction

Carbon nanotubes (CNTs) were discovered in 1991. Structurally, CNTs are graphene sheet rolled, formed by a cylinder of hexagonal rings of carbon atoms[1-2]. There are three types of nanotubes, (1) single wall (SWCNT), these are a graphite sheet rolled like a cylinder and a diameter between 0.5 and 3 nm, (2) double layer (DWCNT), which are constituted by a double layer of graphene sheets with diameters between 1 and 4 nm and, (3) multiple walls (MWCNT), which are concentric cylinders with diameters of 3 to 40 nm[3-5].

CNTs represent one of the most important materials in nanotechnology due to their excellent thermal, physical, chemical, electronic, and mechanical properties[4,6]. Being used for drug delivery systems, biosensors, additives for materials in electronics, optics, the polymer processing industry[7], lithium batteries, cathodes in X-ray equipment, artificial muscles and detection of cancer cells[8]. The various applications of CNTs are attributed to the combination with other materials such as alloys, polymers, fibers or hybrid materials[9]. The introduction of CNTs as reinforcement in a polymer increases the mechanical, electrical, or thermal properties of the polymer in orders of magnitude well above the efficiency of traditional reinforcements due to a homogeneous dispersion of the CNT and an interfacial adhesion with the polymer[10-12]. Some organic polymers that have been reinforced with nanotubes are polyurethane, polyethylene, polypropylene, poly (methyl methacrylate) and polystyrene[13].

In addition, the SWCNT have been used in adsorption processes for the removal of different contaminants due to the size, diameter and distribution in the structure [14-15].

Polyurethane (PU's) represent one of the most versatile materials in the world[16]. They are synthesized by polyaddition polymerization through the interaction between polyols and polyisocyanate[17-18]. PU's contain many urethane groups (–HN–COO–), regardless of the molecular structure[16,19]. An essential characteristic of the PU structure is the microphase separation that arises from the thermodynamic incompatibility between hard and soft segments, so the modification of the PU allows increasing the mechanical properties and thermal stability through the

introduction of an inorganic reinforcement in the PU matrix generating a composite[20].

Composite materials are a combination of specific properties, where the effect of temperature on the diffusion of humidity and environmental ageing represents the main practical repercussion and the influence on solubility, which has established thermodynamic theories.

In recent years, computational simulations using quantum mechanics, molecular dynamics, DFT, and Monte Carlo have been used to analyze the nucleation and growth of SWCNT[21-23]. Computational simulation is an effective area in the energy analysis of small molecules in the gas phase, however, is complicated to determine the mass-energy changes related to infinite structures. Using the technique of grouping the thermochemical properties of various configurations of finite size and extrapolated to an endless length, obtaining global values, for example, that is, there is a comparison of the volume of a specific SWCNT with equal and different chiral vector indices. Therefore, the thermodynamic potentials are obtained. Due to the training of molecular properties at 298K, the PM3 method is helpful in calculating quantities for the important structures[3].

On the other hand, quantitative structure-activity relationships (QSAR) determine the possibility of a relationship between a set of descriptors derived from molecular structure and molecular response; thus, QSAR properties can be considered as a computer-derived rule that describes quantitatively biological activity of chemical descriptors[24].

Monte Carlo simulation allows quantitative study of the effect of temperature on CNT dispersion in a composite material[25-26]. Due to the analysis of the movement of the electron in a random way, where, once an interaction is finished, it is selected by means of another random sample. However, interactions can cause changes in direction, decrease in energy, among others[27]. Although a higher computational cost is required to obtain greater precision in the results[28].

So, the objective was to study, using the PM3 method, the crosslinking of the PU/SWCNT/PMMA nanocomposite. Subsequently, Monte Carlo simulation was used to identify possible changes in the PU/SWCNT/PMMA nanocomposite structure at different temperatures for identifying its possible applications.

2. Materials and Methods

2.1 Computational details

In this study, semi-empirical methods were used to describe the potential energy function of the system. Optimization geometry was calculated using the Hyperchem 8v software on a DELL computer with i7 processor.

PM3 semi-empirical method (Parameterized Model number 3) of quantum mechanics was used applying the conjugate gradient method with the Polak-Ribiere algorithm, 19,000 processing cycles, and an RMS (Root mean square) of 0.001 kcal/(Å-mol) as convergence criteria to obtain the minimum of the potential energy surface (PES) according to the Born-Oppenheimer approximation and the Schrodinger equation[29].

HyperChem software allows to analyze the CNTs[30], and the main physical properties of the PU/SWCNT/PMMA nanocomposite are calculated after Monte Carlo simulation at different temperatures. Thus, the energetic and structural properties were obtained in 20 steps in vacuum mode and varying the temperature.

2.2 Analysis of individual molecules

Geometry optimization is an essential part of computational chemistry. Theoretical research involves calculations of transition structures, heats of formation or vibrational spectra that require searching for one or more minima on a potential energy surface[31]. Figure 1 shows the optimization geometry that determined the location of the atoms in the different molecules[32].

Table 1 shows the energetic properties, where it was observed that the molecules are thermodynamically stable due to a negative Gibbs free energy (ΔG); besides, the SWCNT presented higher ΔG due to the covalent bonds of the sp2 hybridizations[3]. Table 1 shows that SWCNT, PU and PMMA presented a slight change in entropy, related to a slight change in the degree of molecular disorder. Besides was related to the reversibility of the processes because when there is a large molecular disorder passing from one state to another, its reversibility decreases due to heat losses towards the surroundings[33]. Moreover, the dipole moment is a fundamental property of molecules due to the formation of covalent bonds[34]. Thus, the dipole moment values for the SWCNT, PU and PMMA were 3.583, 6.308 and 1.649 Debyes, respectively. This difference in values directly depends on the quantity, type of elements and spatial distribution of the bonds.

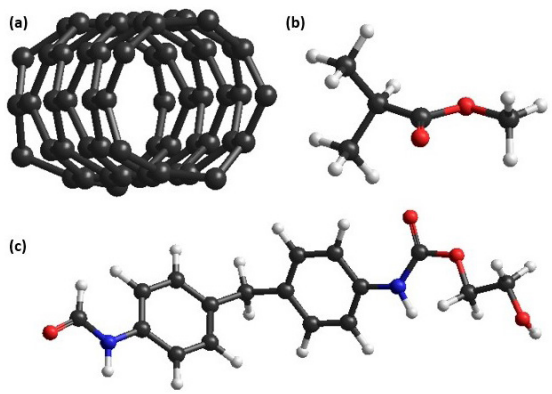

Figure 1. Optimization geometries of individual molecules where (a) SWCNT; (b) PMMA; and (c) PU, where black color: carbon, red color: oxygen, white color: hydrogen, and blue color: nitrogen atoms, respectively.

Table 1. Energetic properties of individual molecules.

Molecule	Gibbs free energy (kcal/mol)	Entropy (kcal/mol)	Dipolar moment (Debyes-D)	Heat of formation (kcal/mol)
SWCNT	– 175599	0.1498	3.583	1822
PU	– 95012	0.1631	6.308	– 115
PMMA	– 32739	0.0919	1.649	– 106

PU has electronegative elements such as oxygen and nitrogen; an irregular and asymmetric geometry was obtained, which produced a higher dipole moment. PMMA showed geometry more compact and regular; however, the electronic distribution presented charges smaller partials. Finally, the SWCNT offered a static dipole moment through the structure of the SWCNT; this dipole moment is inversely proportional to the radius of curvature of the SWCNT and is oriented towards the axis of the tube[35]. The partition coefficient (Log P) is a fundamental molecular descriptor that relates to the bioactivity of compounds or substances[36]; a molecule presents hydrophilic character when Log P<0 and is hydrophobic if Log P>0[37].

Table 2 shows that the three molecules presented hydrophobic character, that is, they are not soluble in water or any polar solvent. Table 2 shows the calculated polarizability values, which indicated that the SWCNT presented higher polarizability due to its molecular structure, and therefore, its dipoles are easily distorted due to the charge transport of its structure[38]. Furthermore, highly polarizable molecules have strong attractions with other molecules[24]. Finally, the surface area and volume calculated for the SWCNT indicated the formation of molecular interactions between the SWCNT with the PU and PMMA, due to the presence of active centers that can react and form a crosslinked.

Figure 2 shows the electronic distribution maps of SWCNT, PU and PMMA, respectively. The distribution of molecular charge obtained from the interaction energy between a unit of positive charge and the distribution of molecular- charge was observed without disturbance[39]. Figure 2a indicated that the SWCNT presented nucleophilic areas (blue color) at the ends of the molecule, and its electrophilic areas (red color) were located in the central part of the tube, which was obtained due to an asymmetry in the superposition of the p orbital, that is, what brings the p-orbital segments located inside the cavity closer together and separates the outer ones.

Therefore, the Coulomb repulsion within the cavity increased with curvature and generated a redistribution of the p orbitals to orbitals intermediate between sp2 and sp3, resulting in an electronic charge transfer from the concave to the convex region[40-41]. Figure 2b-2c show the electrophilic areas around the oxygen atoms, due to tends to gain higher electronic density, mainly a double bond, and nucleophilic zones, which presented a lower electron density around the hydrogen atoms[42].

Table 3 shows the main FTIR vibrations of the SWCNT, PU and PMMA using the PM3method applying a frequency analysis based on the time-independent Schrödinger equation for the stochastic description of the nuclei within the Born-Oppenheimer approximation[43]. The characteristic vibrations of the SWCNT molecule were found to be in the region of 1827 to 1028 cm^{-1} due to symmetric and asymmetric stress[44].

Table 3 shows the FTIR vibrations of the PU where, from 3465 to 3491 cm^{-1} was attributed to the symmetric stretching of the hydroxyl and amino group. A symmetric stretching of the O–H bond was observed at 3491 cm^{-1}, the symmetric stretching of the N–H bond was located in a range of 3465-3449 cm^{-1}, the symmetric stretching of the C–H bond was observed in the range of 3192–2999 and 2926 to 2856 cm^{-1}, from 2035 to 1996 cm^{-1} corresponded to the symmetric stretching of the carbonyl group (C=O), from 1534 to 1378 cm^{-1} was attributed to the symmetric stretching of the C-O bond[45].

Finally, Table 3 (the last column) shows the FTIR vibrations of PMMA where the symmetric stretching of the C–H bond was observed from 3155 to 3022 cm^{-1}, the symmetric stretching of the carbonyl group corresponded of 1527 to 1301 cm^{-1}. Finally, the C-O bond was identified from 1365 to 1301 cm^{-1}[46].

Table 2. QSAR properties of individual molecules.

Molecule	Log P	Polarizability (Å³)	Surface area (Å²)	Volume (Å³)
SWCNT	9.51	107.63	630.94	1308.53
PU	1.80	33.42	574.71	937.27
PMMA	1.05	10.67	286.91	408.67

Table 3. FTIR vibrations of SWCNT, PU and PMMA, respectively.

Bond	Vibration	Wavelength (cm^{-1})		
		SWCNT	PU	PMMA
O–H	Symmetric stretching	---	3491	---
N–H	Symmetric stretching	---	3465–3449	---
C–H	Symmetric stretching	---	3192–2999	---
C–H	Asymmetric stretching	---	3177–3003	3091–3063
C–H	Symmetric stretching	---	3104–3074	3155–3022
C=O	Symmetric stretching	---	2035–1996	2076
C–C	Symmetric stretching	1827–1028	1786–1463	1527–1029
C–C	Asymmetric stretching	---	1792–1749	---
C–N	Symmetric stretching	---	1704–1615	---
C–C	Asymmetric stretching	1690–1199	1617–1576	1440–1215
C–C	Asymmetric stretching	---	1576–1492	---
C–O	Symmetric stretching	---	1534–1378	1365–1301

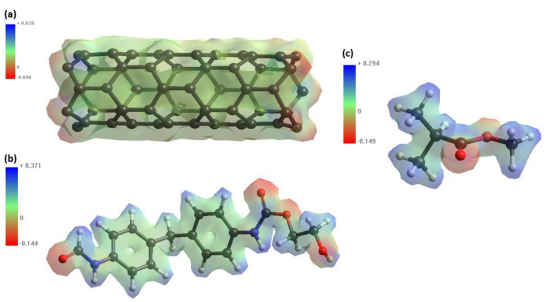

Figure 2. Electronic distribution maps of, (a) SWCNT; (b) PU; and (c) PMMA, where black color: carbon, red color: oxygen, white color: hydrogen and purple color: nitrogen, respectively.

3. Results and Discussions

3.1 Properties of the PU/SWCNT/PMMA nanocomposite

Figure 3 shows the optimized geometry of the PU/SWCNT/PMMA nanocomposite where a crosslinking was observed between the carbonyl groups (PU and PMMA) and the carbon atoms of the central part of the SWCNT. The incorporation of SWCNT in polymers allow the manufacture of polymeric matrix compounds, which are characterized by high mechanical performance and excellent functionality[47-48]. Gibbs free energy obtained for the PU/SWCNT/PMMA nanocomposite was –303323 kcal/mol, that is, there is a spontaneous reaction for the formation of the nanocomposite.

On the other hand, the entropy determined was 0.2826 kcal/mol, that is, greater than that determined for each molecule; besides, this property indicated a decreased reversibility of the nanocomposite formation process, that is, the more energy is lost with the surroundings, the more difficult it is to return to the initial state. Additionally, the nanocomposite presented a dipole moment of 3.9 D, being lower than the individual molecules; that is, the nanocomposite showed more minor asymmetry of electrical charges in chemical bonds due to the best homogeneous distribution of electronic charges. Finally, the heat of formation of the nanocomposite was 1626 kcal/mol; that is, it is an endothermic reaction.

Liao et al applied molecular simulation determinated that in the absence of the atomic bond between the SWCNTs and the polymeric matrix, then electrostatic forces, van der Waals forces or a change in the coefficient of thermal expansion between the SWCNT and the matrix were present, in addition to the groups functional of the SWCNT increased the compatibility with the polymeric matrix

Table 4 shows the calculated results of the QSAR properties of the nanocomposite. It was observed that the positive Log P indicated a hydrophobic character; that is, there will be no tendency to solubility or miscibility in contact with polar substances. The polarizability obtained for the nanocomposite was 147.6 Å^3; this indicated an increase in intermolecular attraction, which influenced in the formation of crosslinking through intermolecular forces such as van der Waals attraction forces.

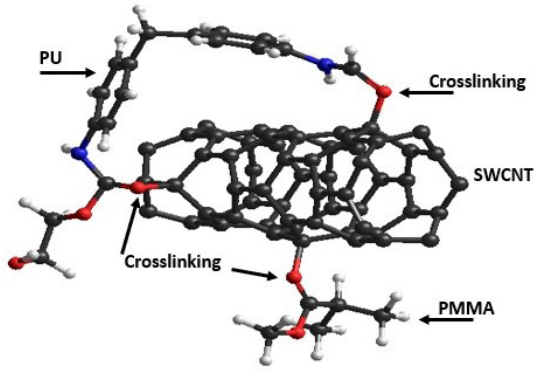

Figure 3. Optimized PU/SWCNT/PMMA composite geometry where: white color: hydrogen, black color: carbon, red color: oxygen and blue color: nitrogen atoms.

Figure 4 shows the MESP of the PU/SWCNT/PMMA nanocomposite, where the electron density distribution can be seen. Besides, the crosslinks between PU/SWCNT and SWCNT/PMMA did not present the formation of molecular orbitals that indicated the presence of any chemical type bond (covalent or ionic bond); therefore the union (crosslinking) between these molecules is the physical type, in addition, when the molecules approach each other, the initial contact produces long-range electrostatic forces[41].

Table 5 shows the FTIR vibrations of the PU/SWCNT/PMMA nanocomposite where, at 1849-1760 and 2058–1755 cm^{-1}, the symmetric stretching of the carbonyl groups were appreciated, the symmetric stretching of the carbonyl groups was appreciated of PU and PMMA, respectively. The symmetric stretching of the C–C bond was observed in the ranges of 1836–1110 and 1673–1019 cm^{-1}. The asymmetric stretching of the C–C bonds corresponded at1729–1130, 1640–1536 and 1367–1023 cm^{-1}. Finally, PU/SWCNT and SWCNT/PMMA crosslinks were observed in the ranges of 1504-1480, 1069-981 and 1069-1043 cm^{-1} which corresponded to the C-O stretching.

3.2 Analysis of the effect of temperature by Monte Carlo simulation

Monte Carlo simulation is a statistical method used to solve mathematical problems through the generation of random variables. Its main objective is to imitate the behavior of real variables to, as far as possible, analyze or predict how they will evolve. This modeling was used to determine the optimized geometries of the PU/SWCNT/PMMA nanocomposite at different temperatures (308.15, 310.15 and 313.15K, respectively) as shown in Figure 5. However, there were no significant changes observed in the nanocomposite's molecular structure, due to the spatial orientation of the atoms and bonds that form the nanocomposite.

Table 6 shows that the Gibbs free energy and heat of formation presented a slight variation concerning the room

Table 4. QSAR properties of PU/SWCNT/PMMA nanocomposite.

Log P	Polarizability (Å^3)	Surface area (Å^2)	Volume (Å^3)
12.14	147.6	1018	2229

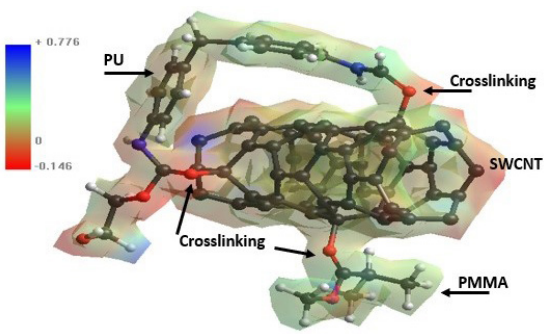

Figure 4. MESP of the PU/SWCNT/PMMA nanocomposite where, white color: hydrogen, black color: carbon, red color: oxygen and blue color: nitrogen atoms. MESP = molecular electrical potential surfaces.

Table 5. FTIR of PU/SWCNT/PMMA nanocomposite.

Wavelength (cm^{-1})	Vibration	Bond (Molecule)
3411	Symmetric stretching	O–H (PU)
3440–3400	Symmetric stretching	N–H (PU)
3191–3164	Symmetric stretching	C–H (PU)
3081–3052, 3042–3009	Asymmetric stretching	C–H (PU, PMMA)
3157–2976, 3106–3067	Symmetric stretching	C–H (PU, PMMA)
2058–1755	Symmetric stretching	C=O (PU, PMMA)
1836–1110, 1673–1019	Symmetric stretching	C–C (PU, SWCNT, PMMA)
1745–1387	Asymmetric stretching	C–C (PU)
1819–1673	Symmetric stretching	C–N (PU)
1729–1130, 1640–1536, 1367–1023	Asymmetric stretching	C–C (PU, SWCNT, PMMA)
1784–1579	Symmetric stretching	C–C (PU)
1675, 1446–1316	Symmetric stretching	C–O (PU, PMMA)
1504–1480, 1069–981	Symmetric stretching	C–O (PU/SWCNT)
1069–1043	Symmetric stretching	C–O (PMMA/ SWCNT)

Table 6. Energetic properties of PU/SWCNT/PMMA nanocomposite determinate by Monte Carlo simulation.

T (K)	Gibbs free energy (kcal/mol)	Entropy (kcal/mol)	Dipolar moment (Debyes)	Heat of formation (kcal/mol)
298.15	– 303324	0.2868	3.657	1625
308.15	– 303221	0.0947	5.893	1728
310.15	– 303215	0.0968	5.741	1734
313.15	– 303212	0.0972	5.127	1737

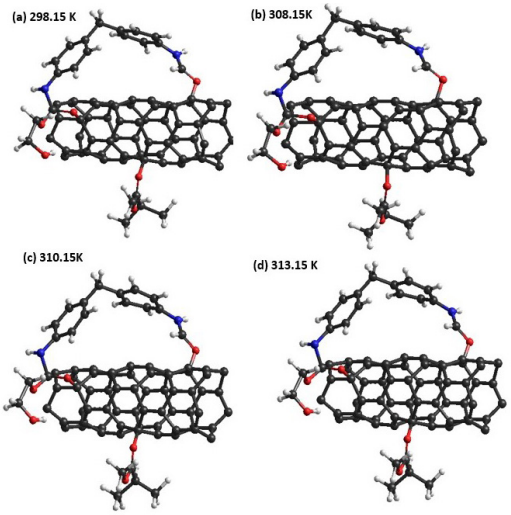

Figure 5. Optimized geometry of the PU/SWCNT/PMMA nanocomposite where: white color: hydrogen, black color: carbon, red color: oxygen and blue color: nitrogen atoms.

temperature (298.15K), being spontaneous and endothermic reactions at these temperatures. On the other hand, the entropy decreased because the structures presented thermodynamic stability attributed to the increase in intermolecular forces by reducing the molecular disorder. Likewise, the dipole moment increased slightly because the electric charge of the dipole moments of the nanocomposites was reorganized due to the orienting effect of the field and temperature.

Table 7 shows the QSAR properties t different temperatures where it was appreciated that there are no noticeable changes in the properties; that is, the difference in temperature will not affect the structure and biological activity of the composite; therefore, the composite will be insoluble in the polar solvent.

Figure 6 shows the electronic and nuclear distribution of the PU/SWCNT/PMMA nanocomposite determined by Monte Carlo simulation at 298.15, 308.15, 310.15 and 313.15K, respectively. Figure 6 showed no changes in the electronic distribution even with the electronic excitation produced by the temperatures; therefore, the PU/SWCNT/PMMA nanocomposite was not affected due to the intermolecular forces of the electrostatic and dipole-dipole type present.

The vibrational frequencies of FTIR at different temperatures are seen in Table 8. After the Monte Carlo simulation, the vibrational and rotational analysis of the nanocomposite was carried out at each of the analysis temperatures to determine if there is any change in absorption frequencies, which would indicate a change in the molecular structure of the nanocomposite since the formation of new bonds caused the displacement towards higher frequency bands

Table 7. QSAR properties of PU/SWCNT/PMMA nanocomposite determinate by Monte Carlo simulation.

T (K)	Log P	Polarizability ($Å^3$)	Surface area ($Å^2$)	Volume ($Å^3$)
298.15	12.14	147.51	1017.81	2228.95
308.15	12.14	147.51	1019.61	2239.35
310.15	12.14	147.51	1018.27	2237.64
313.15	12.14	147.51	1018.07	2233.28

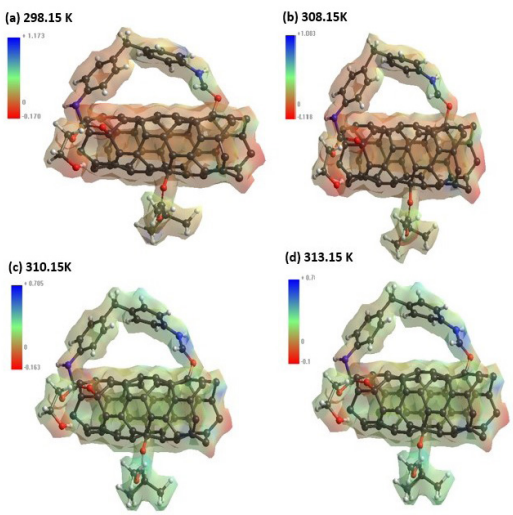

Figure 6. MESP's of the PU/SWCNT/PMMA nanocomposite: (a) 298.15; (b) 308.15; (c) 310.15; and (d) 313.15K. Where: white: H, black: C, red: O and blue: N atoms.

Table 8. Assignment of the FTIR analysis of PU/SWCNT/PMMA nanocomposite by Monte Carlo simulation.

Bond	Vibration	Molecule	Wavelength (cm^{-1})		
			Temperature (K)		
			308.15	310.15	313.15
O–H	Symmetric stretching	PU	3424	3416	3429
N–H	Symmetric stretching	PU	3432–3394	3427–3408	3436–3391
C–H	Symmetric stretching	PU	3183–3158	3177–3149	3032–2997
C–H	Symmetric and asymmetric stretching	PU	3118–3014	3111–3006	3124–2997
C–H	Symmetric and asymmetric stretching	PMMA	3178–2856	3215–2791	3153–2840
C=O	Symmetric stretching	PMMA	2066–1724	2047–1653	2061–1748
C=O	Symmetric stretching	PU	1843–1739	1824–1720	1832–1731
C–C	Symmetric stretching	PU	1819–1156	1779–1184	1803–1239
C–C	Asymmetric stretching	PU	1693–1341	1724–1273	1736–1328
C–C	Symmetric stretching	PMMA	1583–1194	1470–1087	1486–1132
C–N	Symmetric stretching	PU	1835–1745	1816–1658	1844–1663
C–C	Asymmetric stretching	PU	1664–1489	1538–1463	1632–1443
C–C	Asymmetric stretching	SWCNT	1707–1218	1739–1263	1725–1246
C–C	Asymmetric stretching	PMMA	1428–1045	1367–1103	1379–1031
C–C	Symmetric stretching	PU	1761–1483	1820–1517	1753–1456
C–O	Symmetric stretching	PU	1410–1368	1439–1319	1446–1277
C–O	Symmetric stretching	PMMA	1612	1634	1618
C–O	Symmetric stretching	PU/SWCNT	1146–967	1128–1042	1084–976
C–O	Symmetric stretching	PMMA/SWCNT	1083–1010	1114–972	1073–986

as well as the weakening of present bonds to produce band displacements towards lower frequencies[46-48].

4. Conclusions

The SWCNT surface allowed the PU/SWCNT/PMMA crosslinking due to an increase of Van der Waals forces and pi-pi interactions; besides, the adsorption processes were spontaneous and endothermic. QSAR properties indicated a hydrophobic PU/SWCNT/PMMA nanocomposite. FTIR analysis determinate that the crosslink PU/SWCNT and SWCNT/PMMA was due to symmetric stretching of the carboxylic group of the PU and PMMA, respectively.

Monte Carlo simulation indicated that the optimized PU/SWCNT/PMMA nanocomposite geometry was very similar at several temperatures due to the Gibbs free energy had a slight variation, but the reaction was spontaneous and endothermic. Dipole moment increased due to a new orientation of bonds.

Log P showed that the nanocomposite was insoluble in a polar solvent. Finally, FTIR analysis didn't show changes in the absorption frequencies.

5. Author's Contribution

- **Conceptualization –** Juan Ramon Campos-Cruz; Norma Aurea Rangel-Vázquez; Rosa Elvira Zavala-Arce.
- **Data curation** – Juan Ramon Campos-Cruz; Norma Aurea Rangel-Vázquez; Rosa Elvira Zavala-Arce.
- **Formal analysis –** Juan Ramon Campos-Cruz; Norma Aurea Rangel-Vázquez; Rosa Elvira Zavala-Arce.
- **Funding acquisition –** Juan Ramon Campos-Cruz; Norma Aurea Rangel-Vázquez; Rosa Elvira Zavala-Arce.
- **Investigation –** Juan Ramon Campos-Cruz; Norma Aurea Rangel-Vázquez; Rosa Elvira Zavala-Arce.
- **Methodology –** Juan Ramon Campos-Cruz; Norma Aurea Rangel-Vázquez; Rosa Elvira Zavala-Arce; Edgar Marquez-Brazón.
- **Project administration** – Juan Ramon Campos-Cruz; Norma Aurea Rangel-Vázquez; Rosa Elvira Zavala-Arce.
- **Resources** – Juan Ramon Campos-Cruz; Norma Aurea Rangel-Vázquez; Rosa Elvira Zavala-Arce.
- **Software** – Juan Ramon Campos-Cruz; Norma Aurea Rangel-Vázquez; Rosa Elvira Zavala-Arce; Edgar Marquez-Brazón.
- **Supervision** – Juan Ramon Campos-Cruz; Norma Aurea Rangel-Vázquez; Rosa Elvira Zavala-Arce.
- **Validation** – Juan Ramon Campos-Cruz; Norma Aurea Rangel-Vázquez; Rosa Elvira Zavala-Arce.
- **Visualization** – Juan Ramon Campos-Cruz; Norma Aurea Rangel-Vázquez; Rosa Elvira Zavala-Arce; Edgar Marquez-Brazón.
- **Writing – original draft** – Juan Ramon Campos-Cruz; Norma Aurea Rangel-Vázquez; Rosa Elvira Zavala-Arce; Edgar Marquez-Brazón.
- **Writing – review & editing** – Juan Ramon Campos-Cruz; Norma Aurea Rangel-Vázquez; Rosa Elvira Zavala-Arce.

6. Acknowledgements

The authors declare that we have no known competing financial interests or personal relationships that could have appeared to influence the work reported in this paper.

7. References

1. Page, A. J., Ohta, Y., Irle, S., & Morokuma, K. (2010). Mechanisms of single-walled carbon nanotube nucleation, growth, and healing determined using QM/MD methods.

Accounts of Chemical Research, *43*(10), 1375-1385. http://dx.doi.org/10.1021/ar100064g. PMid:20954752.

2. Padilla-Espinosa, I. M., Espinosa-Durán, J. M., & Velasco-Medina, J. (2012). Mecánica molecular estructural para el cálculo del módulo de Young y los modos de vibración de nanotubos de carbono. *Ingeniería y Competitividad*, *14*(1), 91-105. http://dx.doi.org/10.25100/iyc.v14i1.2641.
3. Rodriguez, K. R., Malone, M. A., Nanney, W. A., Maddux, C. J. A., Coe, J. V., & Martínez, H. L. (2014). Generalizing thermodynamic properties of bulk single-walled carbon nanotubes. *AIP Advances*, *4*(12), 127149. http://dx.doi.org/10.1063/1.4905263. PMid:25874156.
4. Díez-Pascual, A. M. (2021). Chemical functionalization of carbon nanotubes with polymers: a brief overview. *Macromol*, *1*(2), 64-83. http://dx.doi.org/10.3390/macromol1020006.
5. Mallakpour, S., & Rashidimoghadam, S. (2019). *Carbon nanotubes for dyes removal*. In G. Z. Kyzas & A. C. Mitropoulos (Eds.), *Composite nanoadsorbents* (pp. 211-243). Amsterdam: Elsevier. http://dx.doi.org/10.1016/B978-0-12-814132-8.00010-1.
6. Lima, A. M. F., Castro, V. G., Borges, R. S., & Silva, G. G. (2012). Electrical conductivity and thermal properties of functionalized carbon nanotubes/polyurethane composites. *Polímeros: Ciência e Tecnologia*, *22*(2), 117-124. http://dx.doi.org/10.1590/S0104-14282012005000017.
7. He, H., Pham-Huy, L. A., Dramou, P., Xiao, D., Zuo, P., & Pham-Huy, C. (2013). Carbon nanotubes: applications in pharmacy and medicine. *BioMed Research International*, *2013*, 578290. http://dx.doi.org/10.1155/2013/578290. PMid:24195076.
8. Reilly, R. M. (2007). Carbon nanotubes: potential benefits and risks of nanotechnology in nuclear medicine. *Journal of Nuclear Medicine*, *48*(7), 1039-1042. http://dx.doi.org/10.2967/jnumed.107.041723. PMid:17607037.
9. Khan, W., Sharma, R., & Saini, P. (2016). *Carbon nanotube-based polymer composites: synthesis, properties and applications*. In M. Berber & I. H. Hafez (Eds.), *Carbon nanotubes - current progress of their polymer composites* (pp. 1-47). London: IntechOpen. http://dx.doi.org/10.5772/62497.
10. Wang, T.-L., Yu, C.-C., Yang, C.-H., Shieh, Y.-T., Tsai, Y.-Z., & Wang, N.-F. (2011). Preparation, characterization, and properties of polyurethane-grafted multiwalled carbon nanotubes and derived polyurethane nanocomposites. *Journal of Nanomaterials*, *2011*, 814903. http://dx.doi.org/10.1155/2011/814903.
11. Chen, W., Tao, X., & Liu, Y. (2006). Carbon nanotube-reinforced polyurethane composite fibers. *Composites Science and Technology*, *66*(15), 3029-3034. http://dx.doi.org/10.1016/j.compscitech.2006.01.024.
12. Sattar, R., Kausar, A., & Siddiq, M. (2015). Advances in thermoplastic polyurethane composites reinforced with carbon nanotubes and carbon nanofibers: a review. *Journal of Plastic Film & Sheeting*, *31*(2), 186-224. http://dx.doi.org/10.1177/8756087914535126.
13. Kalakonda, P., & Banne, S. (2017). Thermomechanical properties of PMMA and modified SWCNT composites. *Nanotechnology, Science and Applications*, *10*, 45-52. http://dx.doi.org/10.2147/NSA.S123734. PMid:28223784.
14. Mykhailenko, O. V., Hui, D., Strzhemechny, Y. M., Matsui, D., Prylutskyy, Y. I., & Eklund, P. (2007). Monte Carlo simulations for carbon nanotubes intercalated with different atomic species. *Journal of Computational and Theoretical Nanoscience*, *4*(6), 1140-1143. http://dx.doi.org/10.1166/jctn.2007.2389.
15. Darkrim, F., & Levesque, D. (1998). Monte Carlo simulations of hydrogen adsorption in single-walled carbon nanotubes. *The Journal of Chemical Physics*, *109*(12), 4981-4984. http://dx.doi.org/10.1063/1.477109.
16. Zia, K. M., Bhatti, H. N., & Bhatti, I. A. (2007). Methods for polyurethane and polyurethane composites, recycling and recovery: a review. *Reactive & Functional Polymers*, *67*(8), 675-692. http://dx.doi.org/10.1016/j.reactfunctpolym.2007.05.004.
17. Alma, M. H., Basturk, M. A., & Digrak, M. (2003). New polyurethane-type rigid foams from liquified wood powders. *Journal of Materials Science Letters*, *22*(17), 1225-1228. http://dx.doi.org/10.1023/A:1025356702660.
18. Wohlleben, W., Meier, M. W., Vogel, S., Landsiedel, R., Cox, G., Hirth, S., & Tomović, Ž. (2013). Elastic CNT–polyurethane nanocomposite: synthesis, performance and assessment of fragments released during use. *Nanoscale*, *5*(1), 369-380. http://dx.doi.org/10.1039/C2NR32711B. PMid:23172121.
19. Xia, H., & Song, M. (2005). Preparation and characterization of polyurethane–carbon nanotube composites. *Soft Matter*, *1*(5), 386-394. http://dx.doi.org/10.1039/b509038e. PMid:32646106.
20. Ali, A., Yusoh, K., & Hasany, S. F. (2014). Synthesis and physicochemical behaviour of polyurethane-multiwalled carbon nanotubes nanocomposites based on renewable castor oil polyols. *Journal of Nanomaterials*, *2014*, 564384. http://dx.doi.org/10.1155/2014/564384.
21. Lobo, L. S., & Carabineiro, S. A. C. (2020). Mechanisms of carbon nanotubes and graphene growth: kinetics versus thermodynamics. *C Journal of Carbon Research*, *6*(4), 67. http://dx.doi.org/10.3390/c6040067.
22. Kato, Y., Inoue, A., Niidome, Y., & Nakashima, N. (2012). Thermodynamics on soluble carbon nanotubes: how do DNA molecules replace surfactants on carbon nanotubes? *Scientific Reports*, *2*(1), 733. http://dx.doi.org/10.1038/srep00733. PMid:23066502.
23. Sankar, R. M., Meera, K. S., Mandal, A. B., & Jaisankar, S. N. (2013). Thermoplastic polyurethane/single-walled carbon nanotube composites with low electrical resistance surfaces. *High Performance Polymers*, *25*(2), 135-146. http://dx.doi.org/10.1177/0954008312459545.
24. Melkemi, N., & Belaidi, S. (2014). Structure-property relationships and quantitative structure-activity relationship modeling of detoxication properties of some 1,2-dithiole-3-thione derivatives. *Journal of Computational and Theoretical Nanoscience*, *11*(3), 801-806. http://dx.doi.org/10.1166/jctn.2014.3431.
25. Haghgoo, M., Ansari, R., Hassanzadeh-Aghdam, M. K., & Nankali, M. (2022). A novel temperature-dependent percolation model for the electrical conductivity and piezoresistive sensitivity of carbon nanotube-filled nanocomposites. *Acta Materialia*, *230*, 117870. http://dx.doi.org/10.1016/j.actamat.2022.117870.
26. Zhu, W., Börjesson, A., & Bolton, K. (2010). DFT and tight binding Monte Carlo calculations related to single-walled carbon nanotube nucleation and growth. *Carbon*, *48*(2), 470-478. http://dx.doi.org/10.1016/j.carbon.2009.09.064.
27. Paro, A. D., Hossain, M., Webster, T. J., & Su, M. (2016). Monte Carlo and analytic simulations in nanoparticle-enhanced radiation therapy. *International Journal of Nanomedicine*, *11*, 4735-4741. http://dx.doi.org/10.2147/IJN.S114025. PMid:27695329.
28. Hasan, S., Guo, J., Vaidyanathan, M., Alam, M. A., & Lundstrom, M. (2004). Monte Carlo simulation of carbono nanotube devices. *Journal of Computational Electronics*, *3*(3-4), 333-336. http://dx.doi.org/10.1007/s10825-004-7071-8.
29. Souza, E. S., Zaramello, L., Kuhnen, C. A., Junkes, B. S., Yunes, R. A., & Heinzen, V. E. F. (2011). Estimating the octanol/water partition coefficient for aliphatic organic compounds using semi-empirical electrotopological index. *International Journal of Molecular Sciences*, *12*(10), 7250-7264. http://dx.doi.org/10.3390/ijms12107250. PMid:22072945.

30. Monajjemi, M., Falahati, M., & Mollaamin, F. (2013). Computational investigation on alcohol nanosensors in combination with carbon nanotube: a Monte Carlo and ab initio simulation. *Ionics*, *19*(1), 155-164. http://dx.doi.org/10.1007/s11581-012-0708-x.
31. Li, X., & Frisch, M. J. (2006). Energy-represented direct inversion in the iterative subspace within a hybrid geometry optimization method. *Journal of Chemical Theory and Computation*, *2*(3), 835-839. http://dx.doi.org/10.1021/ct050275a. PMid:26626690.
32. Schlegel, H. B. (2011). Geometry optimization. *WIREs Computational Molecular Science*, *1*(5), 790-809. http://dx.doi.org/10.1002/wcms.34.
33. Smith, J. M., Van Ness, H. C., & Abbott, M. M. (1997). I*ntroducción a la termodinamica en ingeniería química*. Ciudad de México: McGraw-Hill Interamericana Editores, S.A. de C.V..
34. Gubskaya, A. V., & Kusalik, P. G. (2002). The total molecular dipole moment for liquid water. *The Journal of Chemical Physics*, *117*(11), 5290-5302. http://dx.doi.org/10.1063/1.1501122.
35. Zimmerli, U., Gonnet, P. G., Walther, J. H., & Koumoutsakos, P. (2005). Curvature induced *L*-defects in water conduction in carbon nanotubes. *Nano Letters*, *5*(6), 1017-1022. http://dx.doi.org/10.1021/nl0503126. PMid:15943435.
36. Benfenati, E., Gini, G., Piclin, N., Roncaglioni, A., & Vari, M. R. (2003). Predicting log*P* of pesticides using different software. *Chemosphere*, *53*(9), 1155-1164. http://dx.doi.org/10.1016/S0045-6535(03)00609-X. PMid:14512120.
37. Sawant, P. D., Luu, D., Ye, R., & Buchta, R. (2010). Drug release from hydroethanolic gels. Effect of drug's lipophilicity (log P), polymer–drug interactions and solvent lipophilicity. *International Journal of Pharmaceutics*, *396*(1-2), 45-52. http://dx.doi.org/10.1016/j.ijpharm.2010.06.008. PMid:20540996.
38. Torrens, F. (2004). Effect of size and deformation on polarizabilities of carbon nanotubes from atomic increments. *Future Generation Computer Systems*, *20*(5), 763-772. http://dx.doi.org/10.1016/j.future.2003.11.017.
39. Cruciani, G., Crivori, P., Carrupt, P.-A., & Testa, B. (2000). Molecular fields in quantitative structure–permeation relationships: The VolSurf approach. *Journal of Molecular Structure: THEOCHEM*, *503*(1-2), 17-30. http://dx.doi.org/10.1016/S0166-1280(99)00360-7.
40. Dumitrică, T., Landis, C. M., & Yakobson, B. I. (2002). Curvature-induced polarization in carbon nanoshells. *Chemical Physics Letters*, *360*(1-2), 182-188. http://dx.doi.org/10.1016/S0009-2614(02)00820-5.
41. Chen, S.-Y., Hui, Y., & Yang, Y.-B. (2020). Monte Carlo simulations of adsorption and separation of binary mixtures of CO_2, SO_2, and H_2S by charged single-walled carbon nanotubes. *Soft Materials*, *18*(2-3), 262-273. http://dx.doi.org/10.1080/1539445X.2020.1729806.
42. Cong, Y., & Yang, Z.-Z. (2000). General atom-bond electronegativity equalization method and its application in prediction of charge distributions in polypeptide. *Chemical Physics Letters*, *316*(3-4), 324-329. http://dx.doi.org/10.1016/S0009-2614(99)01289-0.
43. Neugebauer, J., Reiher, M., Kind, C., & Hess, B. A. (2002). Quantum chemical calculation of vibrational spectra of large molecules: raman and IR Spectra for buckminster fullerene. *Journal of Computational Chemistry*, *23*(9), 895-910. http://dx.doi.org/10.1002/jcc.10089. PMid:11984851.
44. Branca, C., Frusteri, F., Magazù, V., & Mangione, A. (2004). Characterization of carbon nanotubes by TEM and infrared spectroscopy. *The Journal of Physical Chemistry B*, *108*(11), 3469-3473. http://dx.doi.org/10.1021/jp0372183.
45. Mondal, S., Memmott, P., Wallis, L., & Martin, D. (2012). Physico-thermal properties of spinifex resin bio-polymer. *Materials Chemistry and Physics*, *133*(2-3), 692-699. http://dx.doi.org/10.1016/j.matchemphys.2012.01.058.
46. Ramesh, S., Leen, K. H., Kumutha, K., & Arof, A. K. (2007). FTIR studies of PVC/PMMA blend based polymer electrolytes. *Spectrochimica Acta. Part A: Molecular and Biomolecular Spectroscopy*, *66*(4-5), 1237-1242. http://dx.doi.org/10.1016/j.saa.2006.06.012. PMid:16919998.
47. Wang, X., Jiang, M., Zhou, Z., Gou, J., & Hui, D. (2017). 3D printing of polymer matrix composites: a review and prospective. *Composites. Part B, Engineering*, *110*, 442-458. http://dx.doi.org/10.1016/j.compositesb.2016.11.034.
48. Cesteros-Iturbe, L. C. (2004). Aplicaciones de la FTIR al estudio de las interacciones polímero-polímero. *Revista Iberoamericana de Polímeros*, *5*(3), 111-132. Retrieved in 2022, September 25, from https://reviberpol.files.wordpress.com/2019/08/2004-cesteros.pdf

Received: May 16, 2022
Revised: Aug. 29, 2022
Accepted: Sept. 25, 2022